

Physical deep learning based on optimal control of dynamical systems

Genki Furuhashi¹, Tomoaki Niiyama², and Satoshi Sunada^{2,3}

¹*Graduate School of Nature Science and Technology,
Kanazawa University*

Kakuma, Kanazawa, Ishikawa, 920-1192, Japan

²*Faculty of Mechanical Engineering,*

Institute of Science and Engineering, Kanazawa University

Kakuma-machi Kanazawa, Ishikawa 920-1192, Japan

³*Japan Science and Technology Agency (JST),*

*PRESTO, 4-1-8 Honcho, Kawaguchi,
Saitama 332-0012, Japan*

(Dated: December 22, 2024)

A central topic in recent artificial intelligence technologies is deep learning, which can be regarded as a multilayer feedforward neural network. An essence of deep learning is the information propagation through the layers, suggesting a connection between deep neural networks and dynamical systems, in the sense that the information propagation is explicitly modeled by the time-evolution of dynamical systems. Here, we present a pattern recognition based on optimal control of continuous-time dynamical systems, which is suitable for physical hardware implementation. The learning is based on the adjoint method to optimally control dynamical systems, and the deep (virtual) network structures based on the time evolution of the systems can be used for processing input information. As an example, we apply the dynamics-based recognition approach to an optoelectronic delay system and show that the use of the delay system enables image recognition and nonlinear classifications, with *only a few* control signals, in contrast to conventional multilayer neural networks which require training of a large number of weight parameters. The proposed approach enables to gain insight into mechanisms of deep network processing in the framework of an optimal control problem and opens a novel pathway to realize physical computing hardware.

PACS numbers:

I. INTRODUCTION

The recent rapid expansion of information technologies, including machine learning, has pushed studies on novel computing concepts and hardware, such as neuromorphic processing [1–6], reservoir computing [7–12], and deep learning [13–16]. In particular, deep learning has been a groundbreaking tool for data processing with the high-level performance [13], and its energy-efficient computing is gaining importance with growing demands for processing a huge amount of data [17].

An underlying key factor of deep learning is its high expressive power induced by the layer-to-layer propagation of information in the deep network to represent highly complex functions in a way that shallow networks with the same number of neurons cannot [18, 19]. Interestingly, recent studies have pointed out that the information propagation in the multilayer systems can be expressed as the time-evolution of dynamical systems [20–23]. From a dynamical system point of view, a learning process of networks can be regarded as optimal control of the dynamical systems [20, 21]. This viewpoint suggests a direct connection between deep neural networks and dynamical systems and indicates the applicability of dynamical systems to physical deep-learning machines.

Herein, we present a novel information processing scheme based on optimal control of continuous-time dynamical systems. For a proof-of-concept, we focus on dynamical systems with delayed feedback and show that delayed feedback enables virtual construction of a deep network structure in a *physically single* node by a time-division multiplexing method. The virtual deep network is based on the time evolution of the systems, which are optimally controlled such that the classification of input data is facilitated, and the classification can successfully be achieved by only a few control signals and minimal weight parameters. The deep network architecture is totally different from other deep learning architectures based on conventional neural networks that require a large number of weight parameters for learning [15, 16]. The proposed scheme is applicable for a variety of experimentally controllable systems and enables easy and large-scale physical implementations of deep networks.

II. MULTILAYER NEURAL NETWORKS AND DYNAMICAL SYSTEMS

First, we briefly discuss the relationship between multilayer neural networks and dynamical systems. Here, let a dataset to be learned be composed by K inputs $\mathbf{x}_k \in \mathbb{R}^M$, $\forall k \in \{1, 2, \dots, K\}$ and their correspondent target vectors, $\mathbf{t}_k \in \mathbb{R}^L$. In supervised learning, the goal is to find a function that maps input vectors onto correspondent targets, $\mathbf{G}: \mathbf{x}_k \rightarrow \mathbf{t}_k$. To this end, we consider an output function $\mathbf{y} = \tilde{\mathbf{G}}(\mathbf{x}, \mathbf{W}) \in \mathbb{R}^L$ parameterized by $\mathbf{W} \in \mathbb{R}^{M_w}$ and the following loss function,

$$J = \sum_k^K \Psi(\mathbf{t}_k, \mathbf{y}_k), \quad (1)$$

where $\Psi(\mathbf{t}_k, \mathbf{y}_k)$ is a function of a distance between the target \mathbf{t}_k and the output $\mathbf{y}_k = \tilde{\mathbf{G}}(\mathbf{x}_k, \mathbf{W})$. \mathbf{W} is determined such that the loss function J is minimized, i.e., the output \mathbf{y}_k corresponds to target \mathbf{t}_k .

As is well-known, a neural network model with a proper activation function is a good candidate to represent the function \mathbf{G} due to its universal approximation capability [24–26]. In multilayer neural networks, the output $\mathbf{y}_k = (y_{1,k}, y_{2,k}, \dots, y_{L,k})^T$ is given by the layer-to-layer propagation of an input \mathbf{x}_k [Fig. 1(a)]. The multilayer network structure based on the layer-to-layer propagation plays a crucial role in increasing the expressivity [18] and enhancing learning performance. In this study, instead of standard multilayer networks, we consider the information propagation in a continuous-time dynamical system,

$$\frac{d\mathbf{r}(t)}{dt} = \mathbf{F}[\mathbf{r}(t), \mathbf{u}(t)], \quad (2)$$

where $\mathbf{r}(t) \in \mathbb{R}^M$ is the state vector in time t , and $\mathbf{u}(t) \in \mathbb{R}^{M_u}$ represents a control signal vector. Based on the correspondence between a multilayer network [Fig. 1(a)] and dynamical model [Fig. 1(b)], we suppose that an input \mathbf{x}_k is set as an initial state $\mathbf{r}(0) = \mathbf{x}_k$ and that the correspondent output \mathbf{y}_k is given by the feedforward propagation of the state vector $\mathbf{r}_k(T) = \mathbf{r}(T, \mathbf{x}_k)$ up an end time $t = T$, i.e., $\mathbf{y}_k = \mathbf{y}[\mathbf{r}_k(T), \boldsymbol{\omega}]$, where $\boldsymbol{\omega} \in \mathbb{R}^{L \times M}$ is a parameter matrix determined in the training process. The loss function J is obtained by repeating the above feedforward propagation for all training data $k \in \{1, 2, \dots, K\}$ and using the output \mathbf{y}_k . The goal of the learning is to find an optimal control $\mathbf{u}^*(t)$ and parameter vector $\boldsymbol{\omega}^*$ such that J is minimized, i.e., $\mathbf{W}^* = (\{\mathbf{u}^*(t)\}_{0 < t \leq T}, \boldsymbol{\omega}^*) = \text{argmin}_{\mathbf{W}} J$. We remark that the learning using the discretized version of Eq. (2) directly corresponds to that using a Residual Network (ResNet) [21, 22].

Because the learning is done by a gradient-based optimization algorithm, the gradients, $dJ/d\mathbf{u}$ and $dJ/d\boldsymbol{\omega}$, are required. $dJ/d\boldsymbol{\omega}$ can be obtained by calculating $\sum_k (\partial J / \partial \mathbf{y}_k \partial \mathbf{y}_k / \partial \boldsymbol{\omega})$. $dJ/d\mathbf{u}$ can efficiently be obtained by the adjoint method developed in the context of optimal control problems as follows,

$$\frac{dJ}{d\mathbf{u}} = \sum_{k=1}^K \mathbf{p}_k^T(t) \frac{\partial \mathbf{F}_k}{\partial \mathbf{u}}, \quad (3)$$

where $\mathbf{F}_k = \mathbf{F}[\mathbf{r}_k(t), \mathbf{u}(t)]$ and $\mathbf{r}_k(t) = \mathbf{r}(t, \mathbf{x}_k)$. $\mathbf{p}_k(t) \in \mathbb{R}^M$ is the adjoint state vector satisfying the end condition at $t = T$, $\mathbf{p}_k(T) = \partial \Psi(\mathbf{t}_k, \mathbf{y}_k) / \partial \mathbf{r}_k|_{t=T}$. For $0 \leq t < T$, the time evolution of $\mathbf{p}_k(t)$ is given by

$$\frac{d\mathbf{p}_k^T(t)}{dt} = -\mathbf{p}_k^T(t) \frac{\partial \mathbf{F}_k}{\partial \mathbf{r}_k}. \quad (4)$$

The derivations of Eqs. (3) and (4) is shown in Appendix A. We note that integrating Eq. (4) in the backward direction (from $t = T$ to $t = 0$) corresponds to the backpropagation in neural networks. In summary, the algorithm for computing optimal \mathbf{u}^* and $\boldsymbol{\omega}^*$ follows:

- (i) Set an input \mathbf{x}_k for the k -th data instance as an initial state, i.e., $\mathbf{r}(0) = \mathbf{x}_k$.
- (ii) Forward propagation: Starting from the initial state \mathbf{x}_k , integrate Eq. (2) and obtain the end state $\mathbf{r}_k(T) = \mathbf{r}(T, \mathbf{x}_k)$. Then, calculate the output $\mathbf{y}_k = \mathbf{y}[\mathbf{r}_k(T), \boldsymbol{\omega}]$.
- (iii) Repeat the forward propagation for all data instances and calculate the loss function J .
- (iv) Backpropagation: Integrate the adjoint Eq. (4) for $\mathbf{p}_k(t)$ in the backward direction from $t = T$ with $\mathbf{p}_k(T) = \partial \Psi / \partial \mathbf{r}_k(T)$.
- (v) Calculate the gradients, $dJ/d\boldsymbol{\omega}$ and $dJ/d\mathbf{u}|_{0 < t < T}$, using Eq. (3).
- (vi) Update control signal $\mathbf{u}(t)$ and parameter $\boldsymbol{\omega}$ based on a gradient-based optimization algorithm.

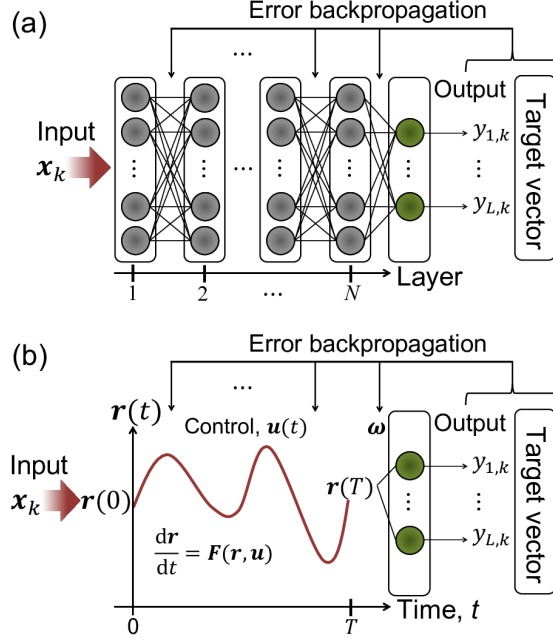


FIG. 1: Schematics of (a) multilayer neural network and (b) dynamical system. In (b), the output $\mathbf{y}_k = (y_{1,k}, y_{2,k}, \dots, y_{L,k})^T$ is given by the end state $\mathbf{r}(T)$ and weight parameter $\boldsymbol{\omega}$. $\mathbf{u}(t)$ and $\boldsymbol{\omega}$ can be updated using a gradient-based optimization algorithm.

A. Binary classification problem

For a brief demonstration, we consider a simple model: $\dot{\mathbf{r}} = \tanh[\mathbf{a}(t)\mathbf{r} + \mathbf{b}(t)]$, where $\mathbf{r} = (\xi, \eta)^T$, and weight $\mathbf{a}(t) \in \mathbb{R}^{2 \times 2}$ and bias $\mathbf{b}(t) \in \mathbb{R}^2$ are used as control signals. We apply this model to a binary classification problem for a spiral dataset, $\{\mathbf{x}_k, c_k\}_{k=1}^K$, where $\mathbf{x}_k \in \mathbb{R}^2$ is distributed around either of two spirals in the $\xi\eta$ -plane, as shown in Fig. 2(a), and \mathbf{x}_k is labeled by c_k as “0” or “1” according to the classes. For the classification, we used one-hot encoding, i.e., the target \mathbf{t}_k corresponding to input \mathbf{x}_k was set as $\mathbf{t}_k = (t_{1,k}, t_{2,k})^T = (1, 0)^T$ if $c_k = 0$ and $\mathbf{t}_k = (0, 1)^T$ if $c_k = 1$. The output $\mathbf{y}_k = (y_{1,k}, y_{2,k})^T$ was set using a softmax function as $y_{l,k} = \exp(z_{l,k}) / \sum_l \exp(z_{l,k})$, where $z_{l,k} = \boldsymbol{\omega}_l^T \mathbf{r}_k(T) + \omega_{l,0}$. $\boldsymbol{\omega}_l \in \mathbb{R}^2$, $\omega_{l,0} \in \mathbb{R}$. If $z_{1,k} \gg z_{2,k}$, \mathbf{y}_k approaches $(1, 0)^T$, whereas if $z_{1,k} \ll z_{2,k}$, \mathbf{y}_k approaches $(0, 1)^T$. The loss function J was chosen as a cross entropy, $J = -\sum_{k=1}^K \sum_{l=1}^2 t_{l,k} \ln y_{l,k}$. Using a training set of $K = 1000$ data points, control signals $\mathbf{u}(t) = \{\mathbf{a}(t), \mathbf{b}(t)\}$ and $\boldsymbol{\omega} = \{\boldsymbol{\omega}_l, \omega_{l,0}\}_{l=1,2}$ were trained such that J is minimized, and the classification accuracy was evaluated using a test set of 1000 data points. For the gradient-based optimization, we used the Adam optimizer [27] with the batch size of K .

Figure 2(b) and 2(c) show the learning curve and classification accuracy for the training and test datasets, respectively, where the loss function monotonically decreases, and the accuracy approaches 100 % classification. For sufficient training over 300 training epochs, the classification accuracy was over 99 % when the end time T is set as $200\Delta t$, where $\Delta t \approx 0.01$ is the time step used in this simulation. Figure 3 shows the time evolution of the two distributions. In the course of the evolution, the distributions of the initial states are disentangled [Figs. 3(a-d)] and becomes linearly separable at the end time T [Fig. 3(d)] to aid the performance of readouts at the output layer. As a result, the input states can be classified into two regions [Fig. 3(e)]. We note that the classification based on the disentanglement is different from that of other models based on dynamical systems, i.e., reservoir computing, where classification is based on mapping of input information onto a high-dimensional feature space [9]. In addition, we note that the disentanglement is facilitated as the end time T is longer, i.e., the number of the layers increases, and high accuracy is achieved up to $T = 600\Delta t$.

III. PHYSICAL IMPLEMENTATION IN DELAY SYSTEMS

In the previous section, we demonstrated a binary classification based on optimal control in a two-dimensional dynamical model, where weight $\mathbf{a}(t) \in \mathbb{R}^{2 \times 2}$ and bias $\mathbf{b}(t) \in \mathbb{R}^2$ were used as control signals. We note that for

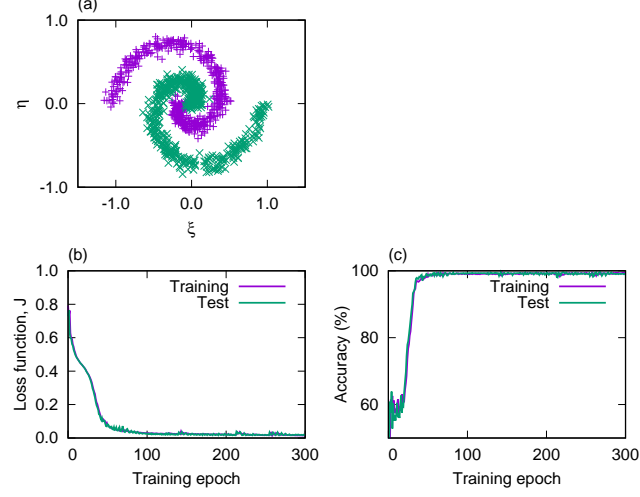


FIG. 2: (a) Spiral dataset for binary classification. (b) Loss function J and (c) classification accuracy as a function of the training epoch.

processing high dimensional data, a high-dimensional dynamical model must be used, and a number of signals used in the dynamical model must be controlled, which will involve a practical difficulty of signal controls in terms of physical implementation in an actual system. In this section, we propose to use a delay system to enable a feasible optimal control. As is known, delay systems can generally be regarded as infinite-dimensional dynamical systems, as visualized in a time-space representation [28], and they can support many virtual neurons by a time-division multiplexing method [10]. In addition, they can exhibit a variety of dynamical phenomena, including stable motion, periodic motion, and high dimensional chaos, with experimentally controllable parameters, i.e., the delay time and feedback strength [29, 30]; thus, we expect their high expressivity.

A. Training based on optimal control in a delay system

Here, we introduce the training method based on optimal control of a delay system, the time evolution of which is governed by the following equation,

$$\frac{d\mathbf{r}(t)}{dt} = \mathbf{F}[\mathbf{r}(t), \mathbf{r}(t - \tau), \mathbf{u}(t)], \quad (5)$$

where $\mathbf{r}(t) \in \mathbb{R}^{M_r}$ and $\mathbf{u}(t) \in \mathbb{R}^{M_u}$ represent the state vector and control signal vector in time t , respectively, and τ is the delay time. The above equation can be integrated by giving $\mathbf{r}(t)$ for $-\tau \leq t \leq 0$ as an initial condition.

The information dynamics can intuitively be interpreted by a space-time representation [28] based on a time discretization of Eq. (5), $\mathbf{r}_n^{j+1} = \mathbf{r}_n^j + \Delta t \mathbf{F}(\mathbf{r}_n^j, \mathbf{r}_{n-1}^j, \mathbf{u}_n^j)$, where $t = n\tau + j\Delta t$, $\mathbf{r}_n^j = \mathbf{r}(n\tau + j\Delta t)$, $n \in \{-1, 0, 1, \dots, N-1\}$, and $j \in \{0, 1, \dots, M-1\}$. In this representation, \mathbf{r}_n^j can be regarded as the j -th network node in the n -th layer, which is affected by an adjacent node \mathbf{r}_n^{j-1} and node \mathbf{r}_{n-1}^j in the $(n-1)$ -th layer, as shown in Fig. 4.

The feedforward propagation is carried out as follows: First, An input $\mathbf{x}_k = (x_{k,1}, \dots, x_{k,M})$ is encoded as $\mathbf{r}_{-1}^j = \mathbf{r}_{-1}^j(x_{k,j})$ for $j \in \{0, 1, \dots, M\}$ in the initial condition. Then, by numerically solving Eq. (5), one can obtain \mathbf{r}_{N-1}^j in the $(N-1)$ -th layer (corresponding to $\mathbf{r}(t)$ for $T - \tau \leq t < T$ in continuous time). The output $\mathbf{y}_k \in \mathbb{R}^L$ is calculated using \mathbf{r}_{N-1}^j . In the continuous time representation, it is defined as $\mathbf{y}_k = \mathbf{y}(\mathbf{z}_k)$, where $\mathbf{z}_k = \int_{T-\tau}^T \boldsymbol{\omega}(t) \mathbf{r}_k(t) dt + \mathbf{b}$. $\boldsymbol{\omega}(t) \in \mathbb{R}^{L \times M_r}$ and $\mathbf{b} \in \mathbb{R}^L$ are the weight and bias parameters to be trained, respectively, and $\mathbf{r}_k(t)$ is the state vector starting from initial state $\mathbf{r}(\mathbf{x}_k)$. Finally, the loss function J [Eq. (1)] is calculated.

For the optimization, the gradients, $dJ/d\mathbf{u}$, $dJ/d\boldsymbol{\omega}$, and $dJ/d\mathbf{b}$ are calculated by the adjoint method as follows:

$$\frac{dJ}{d\mathbf{u}} = \sum_{k=1}^K \mathbf{p}_k^T(t) \frac{\partial \mathbf{F}_k}{\partial \mathbf{u}}, \quad (6)$$

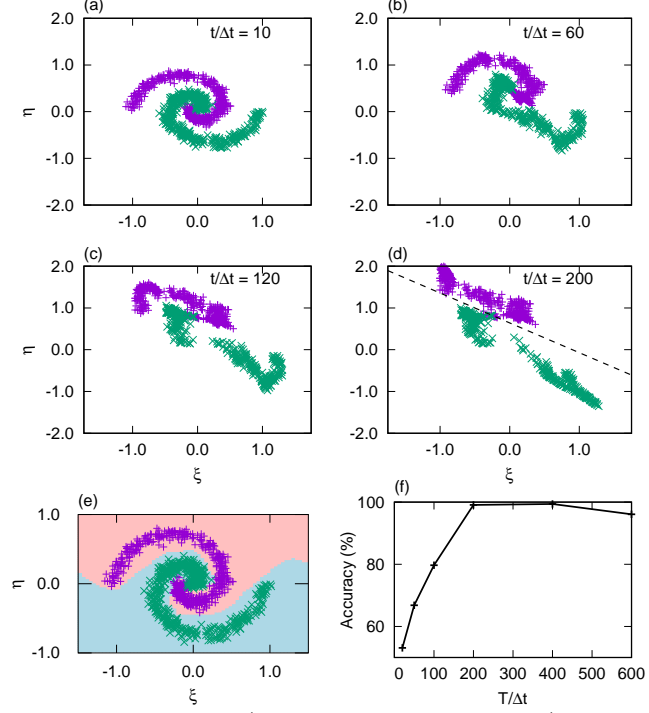


FIG. 3: (a-d) Time evolution of the states in the trained system (at the 300th training epoch) up to the end time $T = 200\Delta t$. $t/\Delta t$ effectively represents the layer number in the viewpoint of a neural network. The initial spiral distribution is disentangled according to the time evolution (layer-to-layer propagation) and becomes linearly separable at the end time $t = T$. In (d), the dotted line represents the decision boundary to separate the two distributions. (e) Result of binary classification. The inputs can be classified into two regions indicated by pink and blue colors. (f) Classification accuracy for a test dataset as a function of the end time T .

$$\frac{dJ}{d\omega} = \sum_{k=1}^K \frac{d\Psi(t_k, \mathbf{y}_k)}{d\omega}, \quad \frac{dJ}{d\mathbf{b}} = \sum_{k=1}^K \frac{d\Psi(t_k, \mathbf{y}_k)}{d\mathbf{b}}, \quad (7)$$

where $\mathbf{F}_k = \mathbf{F}[\mathbf{r}_k(t), \mathbf{r}_k(t-\tau), \mathbf{u}(t)]$. $\mathbf{p}_k(t)$ is the adjoint state vector which satisfies $\mathbf{p}_k(T) = 0$. $\mathbf{p}_k(t)$ can be obtained by solving the adjoint equations in the backward direction. For $T - \tau \leq t < T$, it reads:

$$\frac{d\mathbf{p}_k^T(t)}{dt} = -\frac{\partial \Psi}{\partial \mathbf{z}_k} \omega(t) - \mathbf{p}_k^T(t) \frac{\partial \mathbf{F}_k}{\partial \mathbf{r}_k}, \quad (8)$$

and for $0 \leq t < T - \tau$,

$$\frac{d\mathbf{p}_k^T(t)}{dt} = -\mathbf{p}^T(t) \frac{\partial \mathbf{F}_k}{\partial \mathbf{r}_k(t)} - \mathbf{p}_k^T(t + \tau) \frac{\partial \mathbf{F}_k(t + \tau)}{\partial \mathbf{r}_k}. \quad (9)$$

See Appendix for the details of these derivations.

B. Optoelectronic delay system

As a representative example, we here consider an optoelectronic delay system, as shown in Fig. 5. The delay system is composed of a laser, optoelectronic intensity modulator, photodetector, and electrical filter to construct a time-delay feedback loop. The time-evolution of the system state, $\mathbf{r}(t) = (\xi(t), \eta(t))^T$, is given by the following

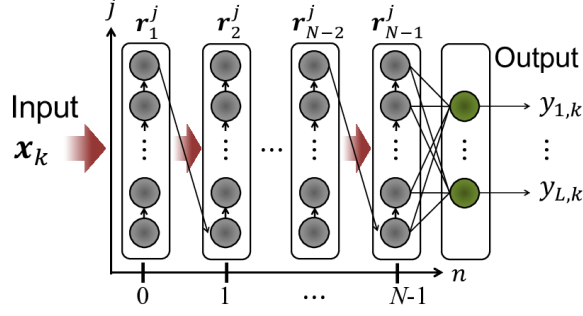


FIG. 4: Schematic of virtual network of a delay system.

equations [31]:

$$\tau_L \frac{d\xi}{dt} = - \left(1 + \frac{\tau_L}{\tau_H} \right) \xi - \eta + \beta \cos^2 [u_1(t)\xi(t-\tau) + u_2(t)], \quad (10)$$

$$\tau_H \frac{d\eta}{dt} = \xi, \quad (11)$$

where $\xi(t)$ is the normalized voltage, and τ_H and τ_L are the time constants of the low-pass and high-pass filters, respectively. In the above, β represents the feedback strength. $u_1(t)$ and $u_2(t)$ are electronic signals added in the feedback loop, which are used as control signals in the system.

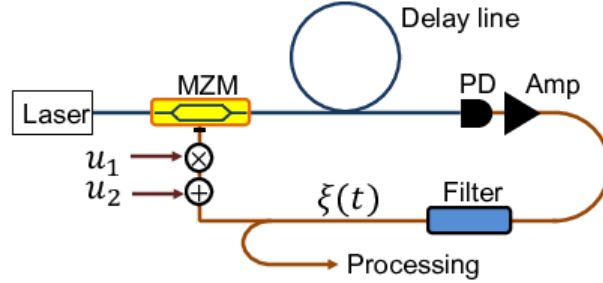


FIG. 5: Schematic of optoelectronic delay system. MZM, Mach-Zehnder modulator; Delay line, optical fiber delay line; PD, photodetector; Amp, electric amplifier; Filter, a two-pole band-pass filter (consisting of low-pass and high-pass filters).

C. Results

1. Binary classification

Here, we demonstrate a binary classification for a spiral dataset, as shown in Fig. 2(a), with the abovementioned optoelectronic delay system. The goal of the binary classification is to classify two categories labeled as “0” or “1” for the spiral dataset. In the same way as shown in Sec. II A, the target \mathbf{t}_k corresponding to input \mathbf{x}_k was set as either of $\mathbf{t}_k = (t_{1,k}, t_{2,k})^T = (1, 0)^T$ or $(0, 1)^T$ based on one-hot encoding. The output $y_{l,k}$ is set as the softmax function, i.e., $y_{l,k} = \exp z_{l,k} / \sum_{l'} \exp z_{l',k}$, where $z_{l,k} = \int_{T-\tau}^T \omega_l(t) \xi_k(t) dt + b_l$, $\omega_l(t) \in \mathbb{R}$ and $b_l \in \mathbb{R}$. Then, the loss function J was defined as the cross entropy $-\sum_{k=1}^K \sum_l t_{l,k} \log y_{l,k}$. In this simulation, most of parameters were fixed as $\tau_H = 1.59$ ms, $\tau_L = 15.9$ μ s, and $\tau = 230$ μ s. The input $\mathbf{x}_k = (x_{k,1}, x_{k,2})^T$ is encoded as the initial state of ξ , i.e., $\xi_k(t) = x_{k,1}$ for $-\tau \leq t < -\tau/2$ and $\xi_k(t) = x_{k,2}$ for $-\tau/2 \leq t \leq 0$. We set $u_1(t) = 1.0$ and $u_2(t) = -\pi/4$ as initial control signals, as shown in Figs. 6(a) and 6(c). For the gradient-based optimization, we used the Adam optimizer [27] with the batch size of K .

In the above condition, the classification accuracy was 99.1% at training epoch 100 when we set the feedback strength $\beta = 3.0$ and end time $T = 5\tau$. To gain insight into the classification mechanism, we investigated the effect of the control signals on the delay dynamics. Figure 6(b) and 6(d) shows the trained control signals $u_1(t)$ and $u_2(t)$, respectively. In Figs. 6(e) and 6(f), we show different instances of $\xi(t)$ starting from three slightly different initial states, in which input values are labeled as “0” or “1” but close to each other. By comparing the instances of $\xi(t)$ before the training [Fig. 6(e)] with that after the training [Fig. 6(f)], we can see that the trajectories starting from initial states with the same label “1” approach each other in the course of the time evolution, whereas the trajectories starting from initial conditions with different labels separate from each other, in particular in a range of $T - \tau \leq t \leq T$, where $\xi(t)$ is used for calculating the output \mathbf{y} . This suggests that the control signals work to aid the separation of two different labeled states for the classification at the output layer.

Figure 7 shows the classification accuracy at training epoch 100 as a function of feedback strength β and end time T/τ . As seen in this figure, classification performance was low for $\beta < 2.0$, where the system exhibits transient behavior to a stable limit cycle motion, which is difficult to control [Figs. 8(a) and 8(b)]. When β increases ($\beta > 2.5$), the system starts to exhibit complex behavior and become sensitive to control signals for a long end time T , as shown in Figs. 8(c) - 8(f). The sensitivity plays a role in aiding the classification; however, too high sensitivity makes it difficult to control the system and decreases the performance due to overfitting, as shown in a range of $\beta > 4.0$ and $T > 7.0\tau$ in Fig. 7. Consequently, high classification performance over 99% is achieved with moderate values of T and β , such that transient behavior around the edge of chaos is used for the classification.

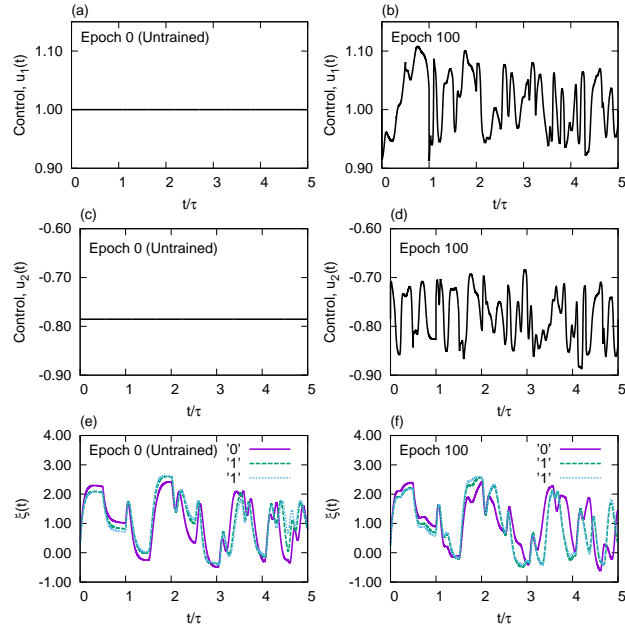


FIG. 6: Control signal $u_1(t)$ (a) at training epoch 0 (before training) and (b) at training epoch 100. Control signal $u_2(t)$ (c) at training epoch 0 (before training) and (d) at training epoch 100. (e-f) Three instances of $\xi(t)$ starting from slightly different initial states, which are labeled as “0” or “1”. The control signals $u_1(t)$ and $u_2(t)$ are trained so as to aid the classification at the output layer.

2. MNIST hand-written digit classification

To investigate classification performance for a higher dimensional dataset, we use the MNIST hand-written digit dataset, commonly used as a standard benchmark for learning [32]. The dataset has a training set of 60,000 28×28 pixel grayscale images of hand-written ten digits, along with a test set of 10,000 images. The initial state, $\xi(t)$, $-\tau \leq t \leq 0$ was set using a one-dimensional vector transformed from an input image, and the delay system was optimally controlled by control signals $\mathbf{u}(t) = (u_1(t), u_2(t))$ [Eqs. (10) and (11)] to obtain the outputs.

Figures 9(a) and 9(b) show the classification accuracy for various values of feedback strength β and delay time τ , where $N = T/\tau = 3$ was fixed. For this image dataset, we found that the delay system with $\beta = 3.0$ exhibits

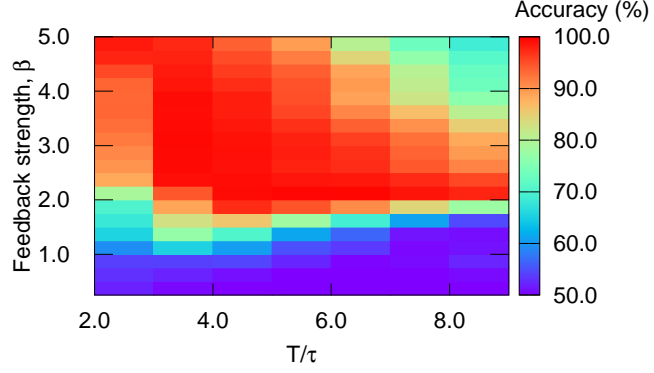


FIG. 7: Classification accuracy as a function of feedback strength β and end time T .

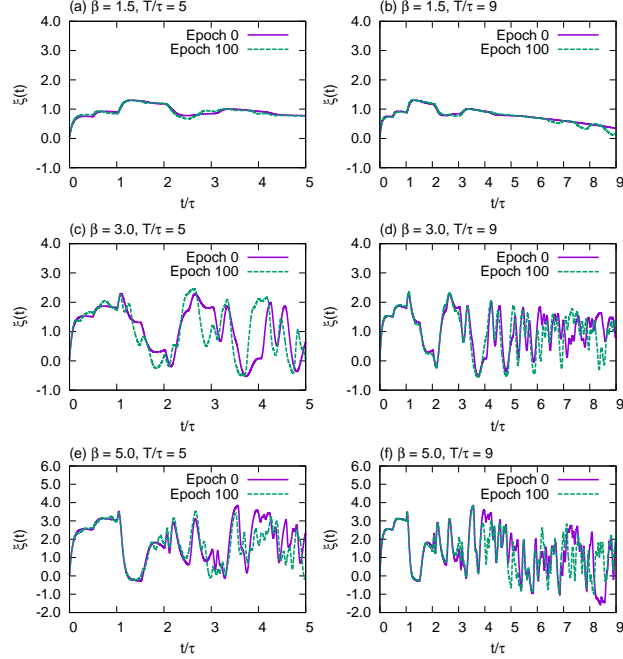


FIG. 8: $\xi(t)$ at training epoch 0 and 100 for various values of β and T .

relatively high classification performance. The best accuracy was 97 % in this delay system. We emphasize that the accurate classification was achieved with a few training signals, $u_1(t)$, $u_2(t)$, $\omega_l(t)$, and b_l , $l \in \{0, 1, \dots, 9\}$, thanks to the time-division multiplexing encoding scheme based on the delay structure, as discussed in Sec. III A. This is totally different from conventional neural networks, where more than hundreds or thousands of weight parameters need to be trained.

We can see that accuracy of the classification can be improved as delay time τ increases [Fig.9(b)]. As discussed in Sec. III A, the effective number of the network nodes M is dependent on τ in this delay system, i.e., $M \approx \tau/\Delta t$, suggesting larger-scale network, i.e., systems with a longer delay, can perform better performance for this large dataset.

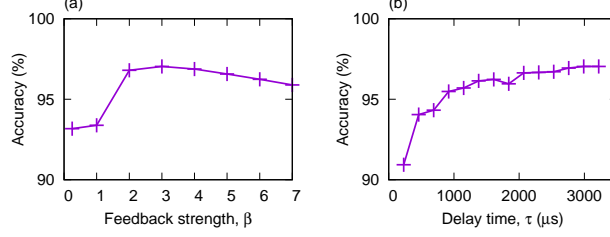


FIG. 9: Accuracy for the MNIST dataset (10,000 test images) as a function of (a) feedback strength β and (b) delay time τ in the delay system, where the end time T was set as 3τ .

IV. SUMMARY AND DISCUSSION

We have proposed and demonstrated novel information processing based on optimal control of dynamical systems. The dynamics-based processing enables to gain insight into the mechanism of information processing based on deep network structures, and it can easily be implemented in physical systems. As a particular example, we have introduced an optoelectronic delay system and have shown that the delay system can be trained to perform nonlinear classification and image recognition with only a few control signals and classification weights, based on the time-division multiplexing method. This is a feature of delay systems, which will be difficult for conventional neural network hardware implementation methods [16]. We emphasize that the dynamics-based processing based on the optimal control is applicable for various physical systems to construct not only feedforward networks but also recurrent neural networks, including reservoir computing, suggesting a novel pathway to physics-based computing.

Acknowledgments

This work was supported, in part, by JSPS KAKENHI (Grant No. 20H042655) and JST PRESTO (Grant No. JPMJPR19M4). The authors thank Profs. Kazutaka Kanno and Atsushi Uchida for valuable discussions on optoelectronic delay systems.

Appendix A: Adjoint method for Eq. (2)

Here, we show the adjoint equations and gradient $dJ/d\mathbf{u}$ used to find an optimal control vector $\mathbf{u}(t)$. The first step is to incorporate the constraint of Eq. (2), $d\mathbf{r}/dt - \mathbf{F}(\mathbf{r}, \mathbf{u}) = \mathbf{0}$, into the loss function J with the Lagrangian multiplier (adjoint) vector $\mathbf{p}_k(t) \in \mathbb{R}^M$ as follows,

$$J_L = \sum_{k=1}^K \left[\Psi(\mathbf{t}_k, \mathbf{y}_k) + \int_0^T \mathbf{p}_k^T (\mathbf{F}_k - \dot{\mathbf{r}}_k) dt \right], \quad (\text{A1})$$

where $\mathbf{r}_k \in \mathbb{R}^M$ is the state vector starting from the initial state $\mathbf{r}_k(0) = \mathbf{x}_k \in \mathbb{R}^M$, and $\mathbf{F}_k = \mathbf{F}(\mathbf{r}_k, \mathbf{u}(t))$. Considering that the second term of Eq. (A1) is rewritten as

$$\begin{aligned} \int_0^T \mathbf{p}_k^T (\mathbf{F}_k - \dot{\mathbf{r}}_k) dt &= -\mathbf{p}_k^T(T) \mathbf{r}_k(T) + \mathbf{p}_k^T(0) \mathbf{r}_k(0) \\ &\quad + \int_0^T (\mathbf{p}_k^T \mathbf{F}_k + \dot{\mathbf{p}}_k^T \mathbf{r}_k) dt, \end{aligned} \quad (\text{A2})$$

we can obtain

$$J_L = \sum_{k=1}^K [\Psi(\mathbf{t}_k, \mathbf{y}_k) - \mathbf{p}_k^T(T) \mathbf{r}_k(T) + \mathbf{p}_k^T(0) \mathbf{r}_k(0)] \\ + \sum_{k=1}^K \int_0^T (\mathbf{p}_k^T \mathbf{F}_k + \dot{\mathbf{p}}_k^T \mathbf{r}_k) dt. \quad (\text{A3})$$

Here, let $\delta \mathbf{r}_k$ and δJ_L be the variations of \mathbf{r}_k and loss function J_L in terms of the variation $\delta \mathbf{u}$, respectively. Then, the variation δJ_L is calculated as follows,

$$\delta J_L = \sum_{k=1}^K \left(\frac{\partial \Psi}{\partial \mathbf{r}_k} \Big|_{t=T} - \mathbf{p}_k^T(T) \right) \delta \mathbf{r}_k(T) \\ + \sum_{k=1}^K \int_0^T \mathbf{p}_k^T \left(\frac{\partial \mathbf{F}_k}{\partial \mathbf{r}_k} \delta \mathbf{r}_k + \frac{\partial \mathbf{F}_k}{\partial \mathbf{u}} \delta \mathbf{u} \right) + \dot{\mathbf{p}}_k^T \delta \mathbf{r}_k dt \\ = \sum_{k=1}^K \left(\frac{\partial \Psi}{\partial \mathbf{r}_k} \Big|_{t=T} - \mathbf{p}_k^T(T) \right) \delta \mathbf{r}_k(T) \\ + \sum_{k=1}^K \int_0^T \left(\mathbf{p}_k^T \frac{\partial \mathbf{F}_k}{\partial \mathbf{r}_k} + \dot{\mathbf{p}}_k^T \right) \delta \mathbf{r}_k dt + \sum_{k=1}^K \int_0^T \mathbf{p}_k^T \frac{\partial \mathbf{F}_k}{\partial \mathbf{u}} \delta \mathbf{u} dt. \quad (\text{A4})$$

Because the Lagrangian multiplier \mathbf{p}_k is free to set, we can choose \mathbf{p}_k such that it obeys the following equation:

$$\mathbf{p}_k^T(T) = \frac{\partial \Psi_k}{\partial \mathbf{r}_k} \Big|_{t=T}, \quad \text{for } t = T \quad (\text{A5})$$

$$\frac{d\mathbf{p}_k^T}{dt} = -\mathbf{p}_k^T \frac{\partial \mathbf{F}_k}{\partial \mathbf{r}_k}, \quad \text{for } 0 < t < T. \quad (\text{A6})$$

In this case, we obtain a simple form of δJ_L as follows, $\delta J_L = \sum_k \int_0^T \mathbf{p}_k^T \frac{\partial \mathbf{F}_k}{\partial \mathbf{u}} \delta \mathbf{u} dt$. Accordingly, when the variation $\delta \mathbf{u}$ is set as $-\alpha \sum_k \mathbf{p}_k^T \frac{\partial \mathbf{F}_k}{\partial \mathbf{u}}$ with a positive constant α , $\delta J_L = -\alpha \int_0^T \delta \mathbf{u}^2 dt \leq 0$ is clearly satisfied, and \mathbf{u} can be updated as the variation by a gradient-based optimization method. Since δJ_L for the variation $\delta \mathbf{u}$ corresponds to the gradient $dJ_L/d\mathbf{u}$, we can express it as follows,

$$\frac{dJ_L}{d\mathbf{u}} = \sum_{k=1}^K \mathbf{p}_k^T \frac{\partial \mathbf{F}_k}{\partial \mathbf{u}}. \quad (\text{A7})$$

Appendix B: Adjoint method for Eq. (5)

Here, we consider the gradient $dJ/d\mathbf{u}$ for the control signals $\mathbf{u}(t)$ in the delay system obeying Eq. (5). In the same way as shown in Appendix A, we consider the loss function J_L incorporating Eq. (5) as follows:

$$J_L = \sum_{k=1}^K \Psi[\mathbf{t}_k, \mathbf{y}_k(\mathbf{z}_k, \boldsymbol{\omega})] + \sum_{k=1}^K \int_0^T \mathbf{p}_k^T (\mathbf{F}_k - \dot{\mathbf{r}}_k) dt, \quad (\text{B1})$$

where $\mathbf{z}_k = \int_{T-\tau}^T \boldsymbol{\omega} \mathbf{r}_k dt + \mathbf{b}$, $\mathbf{F}_k = \mathbf{F}[\mathbf{r}_k(t), \mathbf{r}_k(t-\tau), \mathbf{u}(t)]$, and \mathbf{p}_k is the Lagrangian multiplier (adjoint vector). The variation δJ in terms of the variation $\delta \mathbf{u}$ is described as

$$\begin{aligned} \delta J_L = & \sum_{k=1}^K \left(\frac{\partial \Psi}{\partial \mathbf{z}_k} \int_{T-\tau}^T \boldsymbol{\omega}(t) \delta \mathbf{r}_k dt - \mathbf{p}_k^T(T) \delta \mathbf{r}_k(T) \right) \\ & + \sum_{k=1}^K \int_0^T \mathbf{p}_k^T \left(\frac{\partial \mathbf{F}_k}{\partial \mathbf{r}_k} \delta \mathbf{r}_k + \frac{\partial \mathbf{F}_k}{\partial \mathbf{r}_{k,\tau}} \delta \mathbf{r}_{k,\tau} + \frac{\partial \mathbf{F}_k}{\partial \mathbf{u}} \delta \mathbf{u} \right) dt + \sum_{k=1}^K \int_0^T \dot{\mathbf{p}}_k^T \delta \mathbf{r}_k dt, \end{aligned} \quad (\text{B2})$$

where $\mathbf{r}_{k,\tau} = \mathbf{r}_k(t-\tau)$. In the above equation, considering $\int_0^T \mathbf{p}_k^T(t) \partial \mathbf{F}_k / \partial \mathbf{r}_{k,\tau} \delta \mathbf{r}_{k,\tau} dt = \int_0^{T-\tau} \mathbf{p}_k^T(t+\tau) \partial \mathbf{F}_k(t+\tau) / \partial \mathbf{r}_k \delta \mathbf{r}_k dt$, the variation δJ_L is rewritten as,

$$\begin{aligned} \delta J_L = & - \sum_{k=1}^K \mathbf{p}_k^T(T) \delta \mathbf{r}_k(T) + \sum_{k=1}^K \int_{T-\tau}^T \left(\frac{\partial \Psi}{\partial \mathbf{z}_k} \boldsymbol{\omega}(t) + \mathbf{p}_k^T(t) \frac{\partial \mathbf{F}_k}{\partial \mathbf{r}_k} + \dot{\mathbf{p}}_k^T(t) \right) \delta \mathbf{r}_k dt \\ & + \sum_{k=1}^K \int_0^{T-\tau} \left(\mathbf{p}_k^T(t) \frac{\partial \mathbf{F}_k}{\partial \mathbf{r}_k} + \mathbf{p}_k^T(t+\tau) \frac{\partial \mathbf{F}_k}{\partial \mathbf{r}_k}(t+\tau) + \dot{\mathbf{p}}_k^T(t) \right) \delta \mathbf{r}_k dt + \sum_{k=1}^K \int_0^T \mathbf{p}_k^T(t) \frac{\partial \mathbf{F}_k}{\partial \mathbf{u}} \delta \mathbf{u} dt. \end{aligned} \quad (\text{B3})$$

When $\mathbf{p}_k(t)$ is chosen such that $\mathbf{p}_k(T) = 0$ and the following equations are satisfied,

$$\frac{d\mathbf{p}_k^T(t)}{dt} = -\frac{\partial \Psi}{\partial \mathbf{z}_k} \boldsymbol{\omega}(t) - \mathbf{p}_k^T(t) \frac{\partial \mathbf{F}_k}{\partial \mathbf{r}_k}, \quad \text{for } T-\tau \leq t < T, \quad (\text{B4})$$

and

$$\frac{d\mathbf{p}_k^T(t)}{dt} = -\mathbf{p}^T(t) \frac{\partial \mathbf{F}_k}{\partial \mathbf{r}_k(t)} - \mathbf{p}_k^T(t+\tau) \frac{\partial \mathbf{F}_k(t+\tau)}{\partial \mathbf{r}_k}, \quad \text{for } 0 \leq t < T-\tau, \quad (\text{B5})$$

we can obtain a simple form of δJ_L , as $\sum_{k=1}^K \int_0^T \mathbf{p}_k^T(t) \partial \mathbf{F}_k / \partial \mathbf{u} \delta \mathbf{u} dt$. When $\delta \mathbf{u}$ is chosen as $-\alpha \sum_{k=1}^K \mathbf{p}_k^T(t) \partial \mathbf{F}_k / \partial \mathbf{u}$, $\delta J_L = -\alpha \int \delta \mathbf{u}^2 dt \leq 0$ is always satisfied. In this case, \mathbf{u} can be updated as the variation by a gradient-based optimization method, and we describe the gradient as,

$$\frac{dJ_L}{d\mathbf{u}} = \sum_{k=1}^K \mathbf{p}_k^T \frac{\partial \mathbf{F}_k}{\partial \mathbf{u}}. \quad (\text{B6})$$

1. Adjoint equations in an optoelectronic delay system

In this study, we set the loss function as $J = -\sum_k^K \sum_l^L t_{l,k} \log y_{l,k}$, where $y_{l,k} = e^{z_{l,k}} / \sum_l^L e^{z_{l,k}}$, and $z_{l,k} = \int_{T-\tau}^T \omega_l(t) \xi_k(t) dt + b_l$. In this case, the adjoint equations for $\mathbf{p}_k = (p_{\xi,k}, p_{\eta,k})^T$ are given for $T-\tau \leq t < T$ as follows:

$$\frac{dp_{\xi,k}}{dt} = -\sum_l^L (y_{l,k} - t_{l,k}) \omega_l + g p_{\xi,k} - g_H p_{\eta,k}, \quad (\text{B7})$$

$$\frac{dp_{\eta,k}}{dt} = g_L p_{\xi,k}, \quad (\text{B8})$$

and for $T-0 < t \leq T-\tau$,

$$\frac{dp_{\xi,k}}{dt} = g p_{\xi,k} - g_H p_{\eta,k} + \tilde{\beta} u_1(t+\tau) \sin \delta_k(t+\tau) p_{\xi,k}(t+\tau), \quad (\text{B9})$$

$$\frac{dp_{\eta,k}}{dt} = g_L p_{\xi,k}, \quad (\text{B10})$$

where $g = 1/\tau_H + 1/\tau_L$, $g_H = 1/\tau_H$, $g_L = 1/\tau_L$, $\tilde{\beta} = \beta/\tau_L$, and $\delta_k(t) = 2[u_1(t)\xi_k(t - \tau) + u_2(t)]$. Then, the gradients are given as follows:

$$\frac{dJ}{du_1} = -\tilde{\beta} \sum_k^K p_{\xi,k} \sin \delta_k(t) \xi_k(t - \tau), \quad (\text{B11})$$

$$\frac{dJ}{du_2} = -\tilde{\beta} \sum_k^K p_{\xi,k} \sin \delta_k(t), \quad (\text{B12})$$

and

$$\left(\frac{dJ}{d\omega_l}, \frac{dJ}{db_l} \right) = \left(\sum_k^K (y_{l,k} - t_{l,k}) \xi_k, \sum_k^K (y_{l,k} - t_{l,k}) \right). \quad (\text{B13})$$

-
- [1] D. Marković, A. Mizrahi, D. Querlioz, and J. Grollier, *Nature Reviews Physics* **2**, 499 (2020).
 - [2] M. I. Rabinovich, P. Varona, A. I. Selverston, and H. D. I. Abarbanel, *Dynamical principles in neuroscience*, *Rev. Mod. Phys.* **78**, 1213 (2006).
 - [3] S. Furber, Large-scale neuromorphic computing systems, *J. Neural Eng.* **13**, 051001 (2016).
 - [4] P. A. Merolla *et al.*, A million spiking-neuron integrated circuit with a scalable communication network and interface, *Science* **345**, 668 (2014).
 - [5] J. Feldmann, N. Youngblood, C.D. Wright, H. Bhaskaran, and W. H. P. Pernice, All-optical spiking neurosynaptic networks with self-learning capabilities, *Nature* **569**, 208 (2019).
 - [6] A. N. Tait *et al.*, Neuromorphic photonic networks using silicon photonic weight banks, *Sci. Rep.* **7**, 7430 (2017).
 - [7] D. Verstraeten, B. Schrauwen, M. D’Haene, D. Stroobandt, An experimental unification of reservoir computing methods, *Neural. Netw.* **20**, 391 (2007).
 - [8] H. Jaeger, and H. Haas, Harnessing nonlinearity: predicting chaotic systems and saving energy in wireless communication, *Science* **304**, 78 (2004).
 - [9] G. Tanaka *et al.*, Recent Advances in Physical Reservoir Computing: A Review, *Neural Networks* **115**, 100-123 (2019).
 - [10] L. Appeltant, M. C. Soriano, G. Van der Sande, J. Danckaert, S. Massar, J. Dambre, B. Schrauwen, C. R. Mirasso, and I. Fischer, Information processing using a single dynamical node as complex system, *Nat. Commun.* **2**, 468 (2011).
 - [11] D. Brunner, M. C. Soriano, C. R. Mirasso, and I. Fischer, Parallel photonic information processing at gigabyte per second data rates using transient states, *Nat. Commun.* **4**, 1364 (2013).
 - [12] M. Inubushi and S. Goto, Transfer learning for nonlinear dynamics and its application to fluid turbulence, *Phys. Rev. E* **105**, 043301 (2020).
 - [13] Y. LeCun, Y. Bengio, and G. Hinton, Deep learning, *Nature* **521**, 436 (2015).
 - [14] X. Xu, *et al.* Scaling for edge inference of deep neural networks. *Nat. Electron.* **1**, 216 (2018).
 - [15] X. Lin *et al.*, All-optical machine learning using diffractive deep neural networks, *Science* **361**(6406) 1004-1008 (2018).
 - [16] Y. Shen *et al.*, Deep learning with coherent nanophotonic circuits, *Nat. Photonics* **11**, 441-446 (2017).
 - [17] X. Chen and X. Lin, Big Data Deep Learning: Challenges and Perspectives, *IEEE Access*, **2**, 514 (2014).
 - [18] B. Poole, S. Lahiri, M. Raghu, J. Sohl-Dickstein, and S. Ganguli, Exponential expressivity in deep neural networks through transient chaos, *Adv. Neural. Inf. Process Syst.* **29**, 3360-3368 (2016).
 - [19] F. Montufar, R. Pascanu, K. Cho, and Y. Bengio, On the number of linear regions of deep neural networks, *Adv. Neural Inf. Process. Syst.* **27**, 2924 (2014).
 - [20] G.-H. Liu and E. A. Theodorou, Deep Learning Theory Review: An Optimal Control and Dynamical Systems Perspective, *arXiv:1908.10920v2* (2019).
 - [21] T. Q. Chen, Y. Rubanova, J. Bettencourt, and D. K. Duvenaud, Neural ordinary differential equations, *Adv. Neural. Inf. Process. Syst.*, **31**, 6572-6583 (2018).
 - [22] M. Benning, E. Celledoni, M. J. Ehrhardt, B. Owren, and C.-B. Schönlieb, Deep learning as optimal control problems: models and numerical methods, *arXiv:1904.05657* (2019).
 - [23] E. Haber and L. Ruthotto, Stable architectures for deep neural networks, *Inverse Problems*, **34** 014004 (2017).
 - [24] G. Cybenko, Approximation by superpositions of a sigmoidal function, *Math. Control Signal Systems* **2**, 303 (1989).
 - [25] K. Funahashi, On the approximate realization of continuous mappings by neural networks, *Neural Networks*, **2** 183 (1989).
 - [26] S. Sonoda, and N. Murata Neural network with unbounded activation functions is universal approximator, *Appl. Comput. Harm. Anal.*, **43** 233 (2017).
 - [27] D. P. Kingma and J. Ba, Adam: A Method for Stochastic Optimization, *International Conference on Learning Representations* (2015); *arXiv:1412.6980*.
 - [28] F. T. Arecchi, G. Giacomelli, A. Lapucci, and R. Meucci, Two-dimensional representation of a delayed dynamical system, *Phys. Rev. A*, **45** R4225z(R) (1992).

- [29] A. Uchida, *Optical Communication with Chaotic Lasers* (Wiley-VCH, 2012).
- [30] M. C. Soriano , J. Garcia-Ojalvo, C. R. Mirasso, and I. Fischer, Complex photonic: Dynamics and applications of delay-coupled semiconductor lasers, *Rev. Mod. Phys.* **85**, 421 (2013).
- [31] T. E. Murphy, A. B. Cohen, B. Ravoori, K. R. B. Schmitt, A. V. Setty, F. Sorrentino, C. R. S. Williams, E. Ott and R. Roy, Complex dynamics and synchronization of delayed-feedback nonlinear oscillators, *Phil. Trans. R. Soc. A.* **368**, 343 (2010).
- [32] Y. LeCun, L. Bottou, Y. Bengio, and P. Haffner, Gradient-based learning applied to document recognition, *Proceedings of the IEEE*, **86**, 2278 (1998).